Braced and Urazori Shapes of the Yumi

John C. Neu

April 7, 2024

The question

The aesthetics of the braced yumi's shape is traditionally expressed by "harmonious" geometric proportions of the five curves. The article "Geometry, Aesthetics and the Yumi" presents a specfic proposal for curve proportions connected to Phidia's Golden Ratio. Here, we address a much more pragmatic question: What are the Urazori (reverse curve) shapes of the unbraced yumi corresponding to a prescribed braced shape? Figure 1 shows the braced and unbraced shapes of a Don Symanski Yonsun yumi which is the test case for the analysis presented in this article. Traditionally, the Urazori

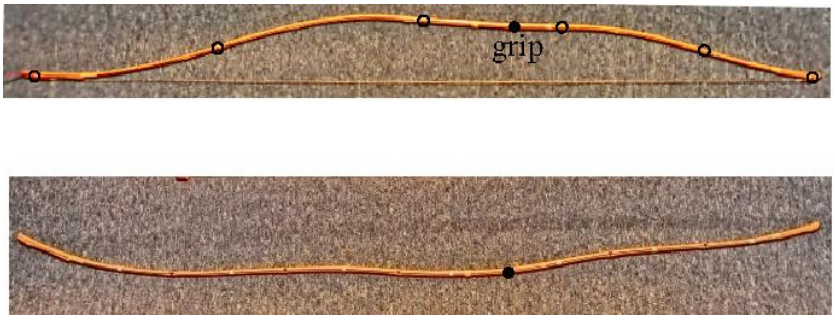

Figure 1: Braced and Urazori shapes of a Don Symanski Yonsun yumi.

shape of a take-yumi made of all natural materials is adjusted by a trial and error process of heat enabled bending. Yumi incorporating modern materials such as carbon laminations between its core and the bamboo back or belly may not be malleable enough for the traditional process. In this case, the correct Urazori shape has to be laminated at the outset. The yumishi needs to know what this shape is.

I. Elastic equilibrium of the braced yumi

Mechanically, a yumi is a thin elastic rod. Our analysis idealizes it as a material plane curve with a specified variation of stiffness along its length. The in-plane assumption is a simplifying approximation. Let $\mathbf{x}(s)$ be the displacement vector from the upper tip to the material point on the yumi at arclength s from the top. The unit tangent to the curve at $\mathbf{x}(s)$ is

$$\mathbf{t}(s) := \dot{\mathbf{x}}(s). \tag{1}$$

The tangent is oriented in the direction, from the upper to lower tip. Let $\theta(s)$

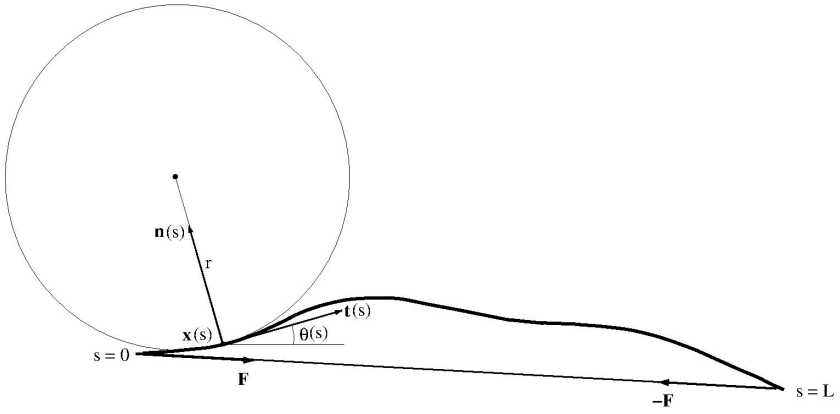

Figure 2: Geometric description of the braced yumi shape.

denote the angle of the tangent $\mathbf{t}(s)$ relative to a fixed direction ("positive horizontal"). The *curvature* of the yumi at $\mathbf{x}(s)$ is defined as $\dot{\theta}(s)$. Figure 2 is the visualization of these definitions for a braced yumi. Short segments of yumi about $\mathbf{x}(s)$ are closely approximated by a circle of radius $1/|\dot{\theta}(s)|$ which "kisses" the yumi at $\mathbf{x}(s)$. This captures the geometric meaning of the curvature's *magnitude*. In general, curvature may be positive or negative. In intervals where the curve bends to the left as we proceed in the direction of its orientation, the curvature is positive, and negative where it bends to the right. Alternatively, the curvature is positive for curves which are convex when viewed from the back, and negative if concave.

For a braced yumi, the tsuru connects the upper and lower tips by a straight line. Letting L_s denote the length of tsuru, we have

$$L_s = |\mathbf{x}(L)|. \tag{2}$$

Here, we have

$$\mathbf{x}(L) = \int_0^L \mathbf{t}(s)ds, \tag{3}$$

where L is the total arclength of yumi. $\mathbf{x}(L)$ is the displacement from the upper tip to the lower. (3) follows by integration of (1) from $s = 0$ to $s = L$. (2) amounts to a *contraint* on possible braced yumi configurations. Since any two configurations related by a translation and a solid body rotation in the plane are physically equivalent, we can fix $\mathbf{x}(L)$ to *one given point* $\mathbf{X}$ on the circle of radius L_s. Hence, we'll work with the constraint

$$\mathbf{x}(L) = \mathbf{X} = given, \tag{4}$$

The physical principle which determines the shape of the bow between given endpoints $\mathbf{x} = 0$ and $\mathbf{x} = \mathbf{X}$ is *energy minimization*: Let $\kappa(s)$ be the curvature of the unbraced bow as a function of arclength s. The *curvature difference* $\dot{\theta}(s) - \kappa(s)$ between braced and unbraced configuations represents actual physical bending which has an energy cost. The elastic energy per unit length is proportional to $(\dot{\theta}(s) - \kappa(s))^2$. This proportionality is elaborated in Landau and Lifshitz "Theory of Elasticity." Details aside, energy per unit length proportional to the square of curvatuve change is intuitively plausible. It is the usual quadratic variation of a function due to small displacements from its minimum. The *elastic energy* stored in the whole bow is

$$E = \frac{1}{2}\int_0^L \mu(s)(\dot{\theta}(s) - \kappa(s))^2 ds. \tag{5}$$

Here, $\mu(s)$ is the *bending modulus* along the length of the bow. It is specified by materials and tapering. Here, we assume it is given. We seek the configuration $\theta = \theta(s)$ which minimizes the energy E subject to the constraint (4). It is sufficient to consider the modified energy

$$\bar{E} := E + \mathbf{F} \cdot (\mathbf{x}(L) - \mathbf{X}), \tag{6}$$

where $\mathbf{F}$ is a two-vector of Lagrange multipliers. Using (3), we may reformulate the modified energy (6) as

$$\bar{E} = \int_0^L \{\frac{\mu}{2}(\dot{\theta} - \kappa)^2 + \mathbf{F} \cdot \mathbf{t}\} ds - \mathbf{F} \cdot \mathbf{X}\, L. \tag{7}$$

The variation of this energy due to variation $\delta\theta$ of θ is

$$\delta\bar{E} = \int_0^L \{\mu(\dot{\theta}-\kappa)\delta\dot{\theta} - \mathbf{F}\cdot\mathbf{n}\,\delta\theta\}ds = \tag{8}$$
$$[\mu\,(\dot{\theta}-\kappa)\,\delta\theta]_0^L + \int_0^L \{-\frac{d}{ds}(\mu(\dot{\theta}-\kappa)) + \mathbf{F}\cdot\mathbf{n}\}\,\delta\theta\,ds.$$

Here, $\mathbf{n}$ is the unit normal of the yumi curve, oriented so $\mathbf{t}$ and $\mathbf{n}$ are a right-handed pair, as in figure 1. We used $\delta\,\mathbf{t} = \mathbf{n}\,\delta\theta$. The vanishing of $\delta\bar{E}$ for all $\delta\theta$ leads to the *elastic boundary value problem* for $\theta(s)$,

$$\frac{d}{ds}(\mu(\dot{\theta}-\kappa)) - \mathbf{F}\cdot\mathbf{n} = 0,\ 0 < s < L, \tag{9}$$
$$\dot{\theta} = \kappa,\ s = 0, L. \tag{10}$$

The boundary conditions (10) express *no bending at the ends*. The two-vector $\mathbf{F}$ of Lagrange multipliers is presumably chosen so the bow shape defined by the solution of (9) and (10) achieves the end to end displacement in (4).

Tsuru tension

The component

$$U := \mathbf{F}\cdot(\mathbf{x}(L) - \mathbf{X}) \tag{11}$$

of the modified energy (6) can be regarded as the potential energy of a particle in a uniform force field $-\mathbf{F}$ at position $\mathbf{x}(L)$. We think of $-\mathbf{F}$ as the *constraint force* required to uphold the prescribed position of the lower tip. $\mathbf{F}$ is proportional to $\mathbf{X}$: Integration of (9) over $0 < s < L$ and use of boundary conditions (10) gives

$$\mathbf{F}\cdot\int_0^L \mathbf{n}ds = 0. \tag{12}$$

We have $\mathbf{n} = J\mathbf{t}$, where J represents counterclockwise rotation of $\pi/2$ radians. Hence

$$\int_0^L \mathbf{n}ds = J\int_0^L \mathbf{t}ds = J\mathbf{X}.$$

Then (12) reduces to $\mathbf{F}\cdot J\mathbf{X} = 0$, which implies the proportionality of $\mathbf{F}$ and $\mathbf{X}$. For braced yumi, the physical agent of the constraint force is the tsuru tension exerted at the lower tip. In this case the constant of proportionality between $\mathbf{X}$ and $\mathbf{F}$ is negative, so $-\mathbf{F}$ points to the upper tip. The upper tip is

subject to the opposite and equal tension $\mathbf{F}$. The tsuru tensions are depicted in figure 2. In other contexts besides yumi, the constant of proportionality between $\mathbf{X}$ and $\mathbf{F}$ may be positive: To straighten a stick bent into the shape of a "U", we can pry the ends apart.

Torque identity

Integration of (9) from $s = 0$ to any s between 0 and L and use of the boundary condition at $s = 0$ gives the identity

$$(\mu(\dot{\theta} - \kappa))(s) = \mathbf{F} \cdot J\mathbf{x}(s). \tag{13}$$

Here, we used

$$\int_0^s \mathbf{n}(s')ds' = J \int_0^s \mathbf{t}(s')ds' = J\mathbf{x}(s).$$

Let us introduce cartesian axes with the upper tip of yumi at the origin,

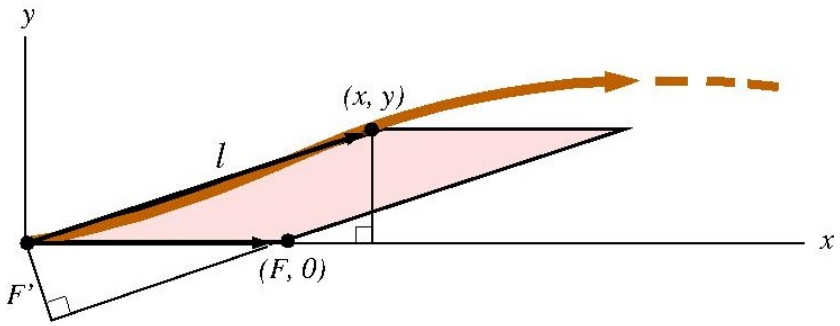

Figure 3: The torque identity

and the lower tip at $(X, 0)$. The tsuru occupies the x-axis between $x = 0$ and $x = X$. The yumi is expected to lie above the x-axis, with elevation $y(s) > 0$ in $0 < s < L$ as depicted in figure 3. In this coordinate description, the tsuru tension is in the positive x direction, and F denotes its magnitude. We have $\mathbf{F} \cdot J\mathbf{x}(s) = -Fy(s)$, and (13) reads

$$(\mu\Delta\kappa)(s) = -Fy(s). \tag{14}$$

Here,

$$(\Delta\kappa)(s) := (\dot{\theta} - \kappa)(s) \tag{15}$$

Geometrically, the $Fy(s)$ is the area of the parallelogram spanned by $\mathbf{F}$ and $\mathbf{x}(s)$: Regarding $\mathbf{F}$ as the base, $y(s)$ is the height and we have area = base $\times$

height $= Fy(s)$. Alternatively, take $\mathbf{x}(s)$ as the base. Let l denote its length. The height is F', the length of $\mathbf{F}$'s projection onto a line perpendicular to $\mathbf{x}(s)$. The area is also represented as $F'l$.

Physically, $-Fy(s) = -F'l$ is the *torque* exerted by the tsuru tension on the limb at $\mathbf{x}(s)$. The minus sign in (14) indicates that this torque acts in a counterclockwise sense. It induces a bending at $\mathbf{x}(s)$ which is convex when seen from the back ($\dot{\theta} - \kappa < 0$). We refer to (14) as the *torque identity*.

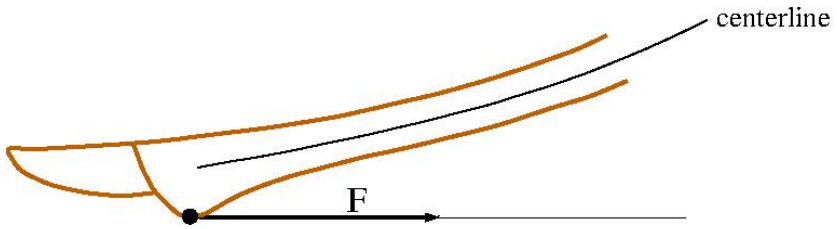

Figure 4: For actual yumi with finite thickness, the tsuru tension acts at a point below the tip of the centerline curve.

This formulation of the torque identity rests on the idealization of the yumi as an elastic material curve of negligible thickness with the tsuru tensions acting on its endpoints. To describe the mechanical equilibrium of a real yumi, we need to acknowledge its finite thickness. We propose a simple model: We idealize the mass and elasticity of the yumi as concentrated along the centerline of its thickness. The tsuru tensions are not exerted at the endpoints of the centerline, but *below* it, as depicted in figure 4. In the torque identity, the elevation profile $y(s)$ of the centerline is not relative to the chord connecting its endpoints, but relative to the *tsuru*.

II. The torque identity informs designs and measurements

In the conventional understanding of the elastic boundary value problem (9), (10), the "knowns" are the bending modulus profile $\mu(s)$ and unbraced curvature profile $\kappa(s)$. The *forward* problem is to solve the elastic boundary value problem (9), (10) for the braced shape and tsuru tension. Our *inverse* problem of determining the unbraced Urazori shape from the braced shape is directly informed by the torque identity. For the moment, let us take the modulus profile $\mu(s)$ as *given*, prescibed by conventional tapering of yumi limbs in both thickness and width. The torque identity (an *integral* of the elastic boundary value problem) specifies the unbraced curvature profile $\kappa(s)$ from the braced curvature and elevation profiles $\dot{\theta}(s)$ and $y(s)$, with the

tsuru tension F as a parameter. The yumishi calculates not one unique unbraced shape, but rather a *family* of candidate shapes with different tsuru tensions F. The Urazori height of each candidate shape is specified by the tsuru tension. In general, we achieve higher tsuru tension by increasing the Urazori height. In practice, the yumishi selects an unbraced shape with Urazori height in the conventional range, $15cm - 20cm$, since yumi with too much Urazori height are prone to flipping when shot.

Before we can implement this design process, we need some quantitative knowledge of the bending modulus $\mu(s)$. Our plan is to "steal" the modulus profile from existing yumi. This stealing is also informed by the torque identity. For a given yumi, both the braced and unbraced shapes are known, along with the braced tsuru tension. In principle, we know the braced elevation profile $y(s)$, the curvature change profile $\Delta\kappa(s)$ and tsuru tension F. Then we solve the torque identity for $\mu(s)$:

$$\mu(s) = -\frac{Fy(s)}{\Delta\kappa(s)}. \tag{16}$$

Simple in principle. The devil is in the details.

III. Mapping a stiffness profile

Measurements of the tsuru tension and elevation profile are straightforward. The first panel of figure 4 depicts the Yonsun yumi braced with a "measurement" tsuru, consisting of two segments of steel cable with a turnbuckle length adjuster and digital scale interpolated in between. The second panel is a close-up of the turnbuckle and scale. When a time dependent force is exerted on the scale, it records the *maximum* force achieved during its application. With a little practice of bracing the yumi with the measurement tsuru, the recorded tension is in fact the static tension F, reproducible in repeated trials. The measured tsuru tension of the Yonsun yumi is 32.05 kg. To measure the elevation profile, replace the measurement tsuru by a regular tsuru adjusted to the same brace height. The regular tsuru presents an unobstructed straight line. The elevation of the yumi center-line above the tsuru is measured in cm with an archery T-square, as depicted in the third panel of figure 5.

Measuring the curvature change profile $\Delta\kappa(s)$ is "meeting the devil in the details." Estimating mathematical derivatives from noisy data is *not* an experimentalist's favorite procedure. Curvature is in essence a *second* derivative and the bamboo surfaces of a yumi are obviously "noisy." Look

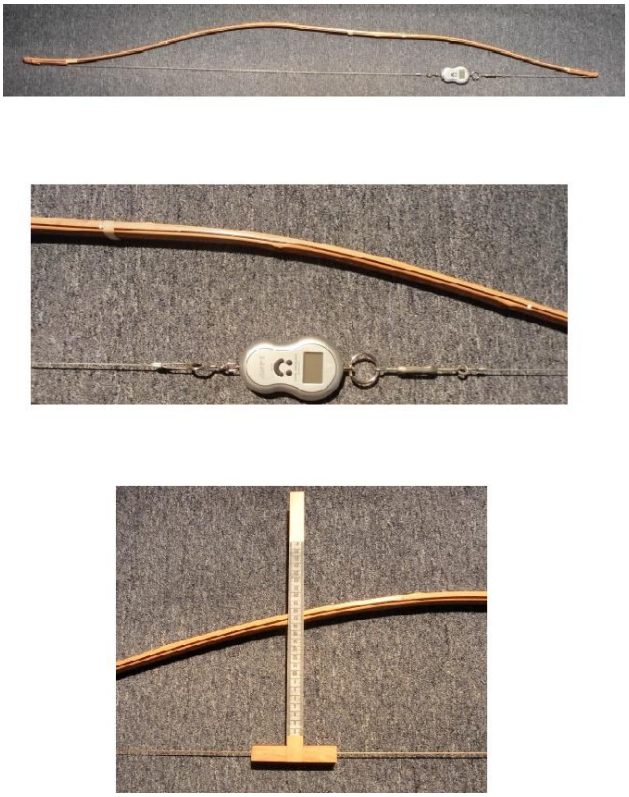

Figure 5: Measuring braced tsuru tension and elevation profile.

at the center-axis of the back: It is close to but not exactly a plane curve, and it has a "rough topography" due to natural features such as the nodal ridges. The mathematical curvature of this center-axis for both unbraced and braced yumi has large fluctuations reflecting this roughness. Fortunately, the effects of this roughness nearly cancel when we examine the *change* in curvature induced by bracing. A "geodesy" visualization helps: Imagine the intersection between a plane of fixed longitude and the surface of the earth as we transect the Himalaya. In figure 6, the smooth arc represents "sea level" and the jagged solid curve, the rough topography of the Himalaya along the line of longitude. Imagine three surveyors at points a, b, c. They can measure the elevation of the line ac as it passes over b. Let a', b', c' be projections of a, b, c down to sea level. Notice that b' is above the line $a'c'$. Later, the curve representing sea level changes due to the movement of the moon. The elevation of b' above the line $a'c'$ changes, reflecting a change in

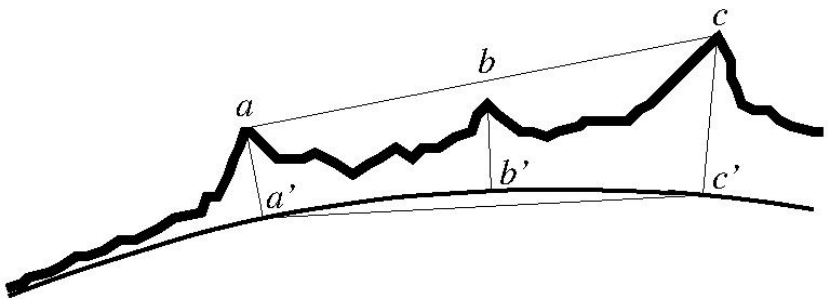

Figure 6: "Geodesy"

curvature of the sea level arc. assuming that the elevations of $a,\ b,\ c$ relative to $a',\ b',\ c'$ remain fixed, the elevation of b relative to the line ac as it passes overhead changes by essentially the same amount. Hence, the surveyors on the rough Himalaya topography can estimate the distortion of the sea level arc. The change in elevation of b relative to the line ac as it passes overhead is proportional to the change in curvature.

Figure 7 depicts the jig which carries out this "geodesy exercise" on the back of a yumi. The jig contacts the yumi's back at three points. Two "right feet" touch down on either side of the center-axis. A prong in between the feet aids centering. The left foot is a spring-loaded screw. The three contact

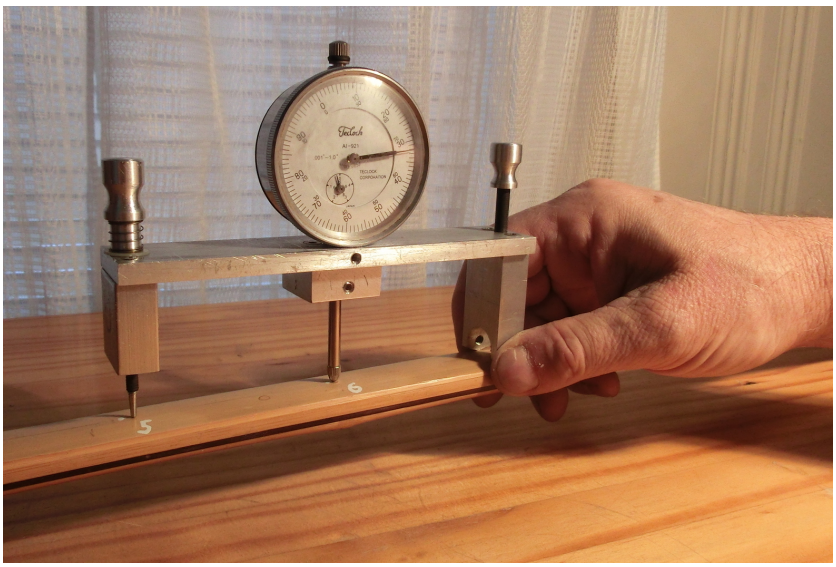

Figure 7: The jig for measuring curvature change due to bracing.

points define a plane, and we measure the elevation of the yumi's back at the halfway mark between the left and right feet, relative to this plane. This is the job of the depth gauge. For instance, suppose the elevation is positive. We "zero" the jig by placing it on a (really) flat surface and turning the spring-loaded screw on the left so the depth gauge plunger just touches the reference flat. Now carefully plant the feet of the jig on a section of yumi back as described before. The depth gauge records a deflection of the plunger in *mills*. (one mill equals one one thousandth of an inch.) If the elevation is negative, we first place the jig on the yumi's back and turn the screw until the depth gauge plunger just touches the yumi. We then place the jig on the reference flat and record the deflection. As in the geodesy example, the change in curvature induced by bracing the yumi is proportional to the change in the elevation. the conversion from elevation change to curvature change is $.00974m^{-1}$ of curvature change for each mill of elevation change. Care is taken so the jig's contact points don't land directly on top of a back node's ridge. For measurement points at a back node, the best "landing point" of the depth gauge plunger is the relatively flat "shelf" adjacent to the sharp ridge. The grip and rattan above the grip are stripped, to get good contact points for the feet of the jig for measurement points near the grip. For each measurement point, we record the curvature change induced by bracing, in m^{-1}.

From the elevation and curvature change at each measurement point and the value of the tsuru tension, we calculate corresponding bending modulii from the torque identity (14). The horizontal axis of figure 8 is arc length along the yumi measured from the upper tsuru nock in cm. The vertical axis is bending modulus in $kg\ m^2$. The diamonds represent measurement points centered at nodes, circles, measurement points between nodes. The error bars are based on common-sense estimates of measurement uncertainties: The archery T-square depicted in figure 4 is marked in millimeter increments, so we allow $.1cm$ error in the sampling of the elevation profile $y(s)$. The depth gauge in figure 7 is marked in $1\ mill = .001$" increments. In practice, repeated measurements using the jig in figure 7 on the back of a yumi show typical variations two times bigger, or $2\,mill$. The corresponding uncertainty in the measured curvature change $\Delta\kappa$ is $.02m^{-1}$. Since bending modulus is proportional to the quotient of elevation and curvature change, the uncertainty in modulus due to uncertainties in elevation and curvature change acting independently is easily estimated, and that is what sets the lengths of the error bars in figure 8.

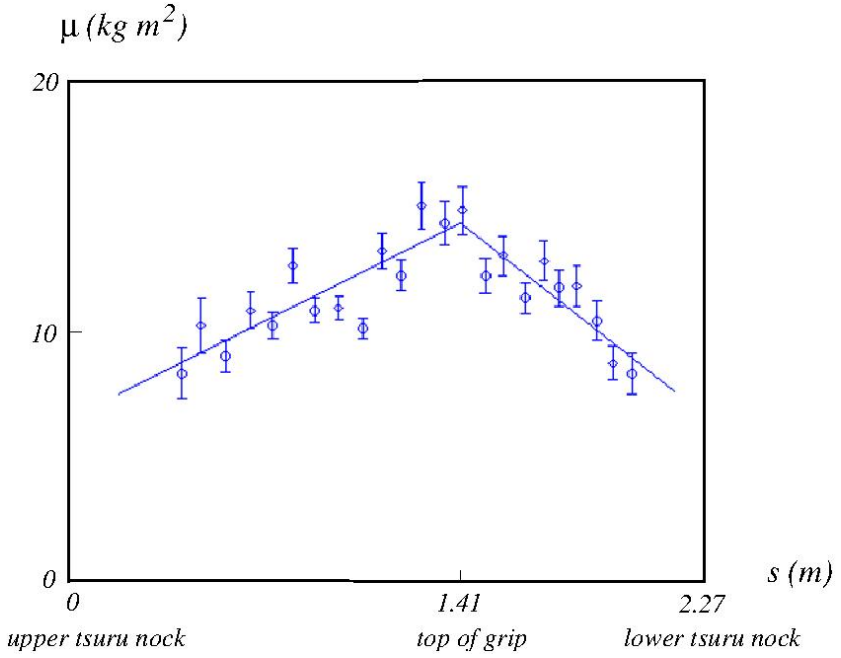

Figure 8: Measured modulus profile of Don Symanski Yonsun yumi.

The data has significant scatter. We don't explain it away as pure measurement uncertainty. The error bars are too small for that. Most likely, non-uniformity of the natural materials in the yumi is involved, especially variation of the bamboo skins along their lengths. Recall that diamonds in the graphs of figure 8 correspond to measurement points at nodes, circles to measurement points between nodes. Imagine connecting the diamonds by a piecewise line. Almost all of the circles lie below it. It appears that nodes induce extra stiffness.

Underlying the scatter, there is a gradual decrease of the modulus as we move from the grip to the ends. In figure 8, we've plotted line segments that are least squares fits of the modulus data above and below the grip. The least squares line segments almost join at the grip. The line segments are not continued into the intervals near the ends where the strike plates are. Strike plates induces enormous stiffness so there is essentially no bending of the limb under a strike plate. The stiffnesses when we reach the strike plates is roughly half of the stiffness at the grip. In design calculations of the Urazori shape from the braced shape, we use the simple piecewise linear approximation to the modulus profile. We will need quantitative details: The

first column of table 1 records the *slopes* of the lines in intervals of arc length above and below the top of the grip.

Table 1: Piecewise linear modulus profile

intervals	slopes ($kg\ m$)	intercepts $kg\ m^2$)
above	.0546	14.35
below	$-.0812$	14.24

IV. Urazori shape from braced shape

In section II we give the broad outline of determining the Urazori shape of the yumi from its braced shape. The braced elevation profile $y(s)$, the braced curvature profile $\theta(\dot{s})$ and the modulus profile $\mu(s)$ are inputs for this determination. For the modulus profile, we adopt the piecewise linear approximation just discussed. For the braced elevation and curvature profiles, we use proxies based on the lengths and depths of the five curves as described in the article, "Geometry, Aesthetics and the Yumi."

We recall that the endpoints of curves are *inflection points* where the curvature vanishes. In the photograph of the braced Don Symanski Yonsun in figure 1, these are marked by hollow dots. The four interior inflection points are located by sighting along the length of the yumi to detect transitions between concavity and convexity. We take the upper and lower tips to be inflection points as well: The shape of the uncured yumi lamination is imposed by applying some force profile (the clamps) along it. *Finite* forces cannot change curvatures of laminations at their very tips. Since the laminates before lay up are close to straight, we expect negligible curvature at the tips.

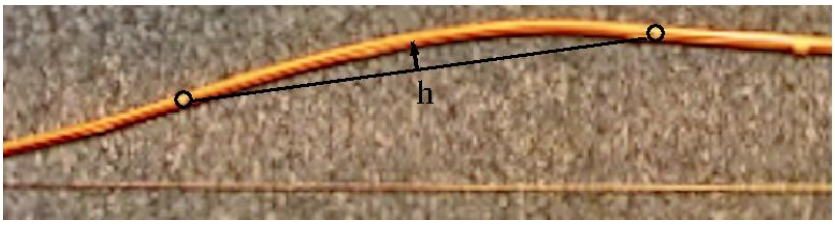

Figure 9: The depth of a curve

We recall the definition of a curve's *depth*. The line segment connecting its endpoints is called its chord. The depth of the curve is its largest perpendicular displacement from the chord. We reckon the depth *positive* for curves which are convex when viewed from the back, and *negative* if concave. In the closeup of figure 9, we've drawn the chord of the second curve from the top and indicated the perpendicular displacement which defines its depth. Table 2 lists the lengths l and depths h of the five curves of the Don Symanski Yonsun yumi, from top to bottom. To measure the depth of a curve, we physically realize its chord by a taut thread between its endpoints. The perpendicular displacement from this thread to the yumi centerline is measured with digital calipers.

Table 2: Lengths and depths of the Yonsun curves.

$l\ (cm)$	$h\ (cm)$
55.5	-2.90
57.8	$+3.56$
37.2	$-.40$
48.8	$+2.27$
28.0	$-.64$

We approximate the curve between its endpoints by a *trigonometric spline*. For a curve with length l with its midpoint at arc length $\bar{s}$, the spline approximation to curvature takes the form

$$\dot{\theta}(s) = K\cos(\pi\frac{s-\bar{s}}{l}),\ |s-\bar{s}| < \frac{l}{2}. \tag{17}$$

The curvature of the spline vanishes at its endpoints as it should, since curve endpoints are inflection points. The *curvature amplitude* K is related to the depth of the spline. If we orient the spline so its tangent at its midpoint is horizontal ($\theta(\bar{s}) = 0$), integration of (17) gives

$$\theta(s) = \frac{Kl}{\pi}\sin(\pi\frac{s-\bar{s}}{l}). \tag{18}$$

The depth of the spline is

$$-\int_{\bar{s}}^{\bar{s}+\frac{l}{2}} \sin\theta(s)ds.$$

The minus sign is consistent with the convention, that the sign of the depth is opposite the sign of the curvature. We identify the spline depth with the measured curve depth, so

$$h = -\int_{\bar{s}}^{\bar{s}+\frac{l}{2}} \sin\theta(s)ds. \tag{19}$$

Substituting (18) for $\theta(s)$, we see that h is a function of K. In practice, yumi curves are shallow, with $Kl << 1$, and (19) asymptotically reduces to

$$h \sim -\frac{Kl^2}{\pi^2}. \tag{20}$$

Approximating K in terms of h according to (20), (17) takes asymptotic form

$$\dot{\theta}(s) \sim -\frac{\pi^2 h}{l^2}\cos(\pi\frac{s-\bar{s}}{l}),\ |s-\bar{s}| < \frac{l}{2}. \tag{21}$$

For each curve, we can determine a spline which matches it in length and depth. Given the individual splines of all five curves, we join them smoothly end to end in the proper order to approximate the yumi shape. In figure 10, the green curve is the spline approximation of the Don Symanski Yonsun based on the curve lengths and depths in table 2. We've super-positioned it over the actual braced shape. The deviation we see in figure 10 has a

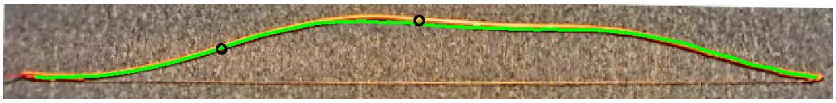

Figure 10: Spline approximation to the Symanski Yonsun.

physical significance. The two hollow dots mark the endpoints of the second curve from the top. We see that the right side of this curve bulges out, and so deviates from the spline of that curve. Splines are symmetric about their midpoints. One might suspect that the right portion of the second curve is a weak section of this yumi. Now look back at figure 8 with its plot of the modulus data. Specifically, look at the fifth data point above the grip.

The design calculation

We outline the practicalities of a design calculation. The inputs are the lengths and depths of the five curves of the braced yumi, the piecewise linear

profile of the bending modulus, and the tsuru tension. The proxy for the braced curvature profile $\dot{\theta}(s)$ is the trigonometric spline approximation (21). The curvature profile of a yumi determines its shape, modulo its orientation in the plane. For the moment, assume that the upper tip is horizontal, so the angle profile which follows by integration of curvature is

$$\theta(s) = \int_0^s \dot{\theta}(s')(s')\, ds'. \tag{22}$$

The parametric equations of the braced shape with the upper tip at $(x, y) = (0, 0)$ are

$$x(s) = \int_0^s \cos\theta(s')\, ds', \;\; y(s) = \int_0^s \sin\theta(s')\, ds'. \tag{23}$$

We rotate and translate this shape so the upper and lower tips have the proper distances above the x-axis which represents the line of the tsuru. The resulting $y(s)$ is the spline approximation to the yumi centerline's elevation profile above the tsuru. The unbraced curvature $\kappa(s)$ is determined from the torque identity in the form

$$\kappa(s) = \dot{\theta}(s) + \frac{Fy(s)}{\mu(s)}. \tag{24}$$

The tsuru tension is an adjustable parameter. The shape of the unbraced yumi follows by repeating the construction (22), (23) with the unbraced curvature $\kappa(s)$ replacing the braced curvature $\dot{\theta}(s)$. Specifically, the angle profile of the unbraced yumi is

$$\Theta(s) = \int_0^s \kappa(s')\, ds'. \tag{25}$$

and the parametric equations (23) of the shape are recomputed with $\Theta(s)$ in place of $\theta(s)$. We may rotate the unbraced shape so its tips lie on the x-axis.

For numerical work, we adopt mesh values of the arc length s which divides each of the five curves into eight equal intervals. Mesh values of the braced curvature $\dot{\theta}(s)$ follow by evaluating the trigonometric spline approximation (21) at mesh points. The integrals (22), (23) are approximated by the trapezoid rule. From mesh values of braced elevation profile $y(s)$ and bending modulus profile $\mu(s)$, we determine mesh values of the unbraced curvature profile $\kappa(s)$ from the torque identity (24). We repeat the numerical construction of the yumi shape from its curvature, this time using mesh values of the unbraced curvature.

A test case

We test the design calculation on the Symanski Yonsun, for which the braced and Urazori shapes, the modulus profile and braced tsuru tension are all known. We've already computed the spline approximation to the braced shape based on the curve lengths and depths in table 2, and compared it to the actual braced shape (figure 10). We obtain the inputs for the calculation of the unbraced shape. In particular, the yumi centerline elevations above the tsuru at both tips are measured. Both are close to 1.5 cm. The spline approximation to the braced shape is placed so its tips are 1.5 cm above the tsuru. This specifies the braced elevation profile $y(s)$. In figure 11, the green curve representing the computed unbraced shape is super-positioned over the actual unbraced shape in the photograph.

Figure 11: The design calculation of the unbraced shape (green curve) closely matches the actual unbraced shape. Some details: The braced tsuru tension that goes into this calculation is the measured value, 32.05 kg. The 1.5 cm elevation of the braced yumi centerline above the tsuru at the tips is important. If we neglect it, the computed Urazori shape is shallower by roughly 2 cm over much of the yumi's length.

V. The multiplicity of Urazori shapes

The blue curve in the top panel of figure 12 is the spline approximation to the shape of the braced Symanski Yonsun. The magnta curves are computed Urazori shapes corresponding to the sequence of braced tsuru tensions,

$$24\ kg, 28\ kg, 32\ kg, 36\ kg, 40\ kg, 44\ kg. \tag{26}$$

We've highlighted the Urazori shape corresponding to brace tension 32 kg, which is close to the measured value for the Symanski Yonsun. Define the *Urazori depth* as the greatest perpendicular displacement of the shape curve from the chord line between its tips.. The second panel of figure 12 plots the Urazori depth versus brace tension. The graph quantifies the intuition, of the brace tension increasing with the Urazori depth. Traditionally, the Urazori depth is in the range 15 $cm - 20\ cm$. Yumi with exessive Urazori depth

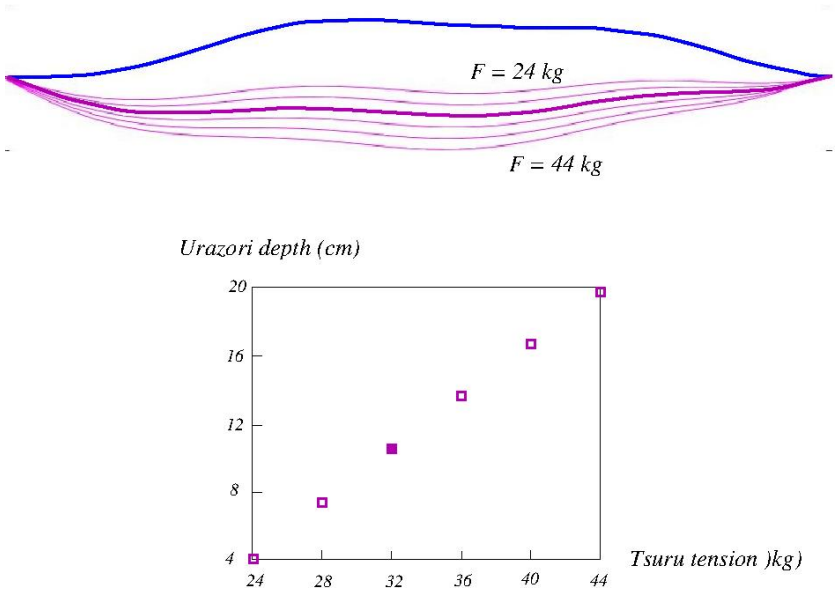

Figure 12: Top panel: The braced shape of the Symanski Yonsun (blue) and a sequence of Urazori shapes (magenta) corresponding to it. Second panel: Urazori depth versus the brace tension it induces.

are prone to out of plane flipping. In a design calculation, one can adjust the braced tsuru tension in order to achieve a prescribed Urazori depth near 15 cm.

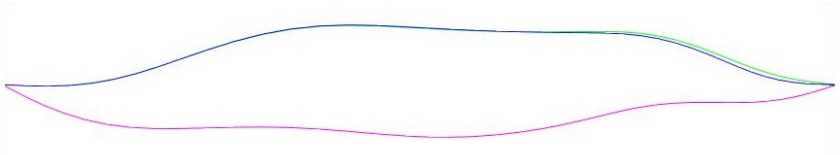

Figure 13: The blue curve is an original "mirror symmetry" shape, which is nearly tangent to the tsuru at the lower tip. The green curve is a "broken mirror symmetry shape" which opens the angle between yumi and tsuru at the lower tip. The magenta curve is the "broken mirror symmetry" Urazori shape whose depth is 15 cm.

In "Geometry, Aesthetics and the Yumi," we formulated "broken mirror symmetry" curve proportions. The blue curve in figure 13 is an original "mirror symmetry" shape reproduced from figure 9 of that article. Unlike

the shapes of most real yumi, the tangent to the shape at the lower tip is almost parallel to the tsuru. The green curve in figure 13 is a "broken mirror symmetry" shape. Its bottom curve is straighter, which opens up the angle between the yumi and tsuru at the bottom tip. The concavity of the middle curve is increased so as to preserve the brace height (Ha) close to 15 cm. Finally, the magenta curve is an Urazori shape which corresponds to the braced "broken mirror symmetry" shape. The Urazori depth is chosen to be 15 cm. The layup of this Urazori shape in the shop is now the yumishi's problem.